

TS-Fuzzy Controllers based Vector Control of Induction Motor for Water Pumping System fed by Hybrid Standalone PV-Wind-Battery

Vaibhavi M. Parmar^{*1}, Dharmishta V. Makwana², Nilam B. Panchal³, Mehulsinh G. Jadeja⁴, Rinal K. Ahir⁵, Vaishali K. Patel⁶

Submitted: 28/01/2024 Revised: 06/03/2024 Accepted: 14/03/2024

Abstract: Water pumping systems play a vital role in modern daily activities and can reduce pollution by utilizing renewable energy sources. Implementing standby power using hybrid renewable sources can ease peak demand on the electric grid. Common sources include wind and photovoltaic systems, requiring energy storage due to their intermittent nature. Integrating batteries and converters ensures uninterrupted water supply. Installing generators on water tanks or buildings in urban or rural areas optimizes space. However, efficient operation requires coordinated energy management. A proposed centralized approach employs PMDC generators for wind and induction motors for pumps. Maximum power point trackers optimize energy utilization, with a bidirectional dc-dc circuit regulating battery voltage. Sensor less vector control and Takagi Sugeno Fuzzy controllers enhance system efficiency, demonstrated using OPAL-RT Hardware-in-Loop systems. This approach aims to optimize water pumping efficiency while reducing reliance on the electric grid in both urban and rural areas with limited space.

Keywords: Induction Motor Drive, Direct Torque Control, LSTM-ANN Controller, Space Vector Modulation

1. Introduction

Water is an essential resource for fulfilling daily activities. To bring water from underground to the point of use, a pump is necessary. In many areas, overhead tanks are constructed to store water and ensure a steady supply according to demand. Additionally, separate tank systems are built in apartments to meet the residents' daily water needs. These water tanks are usually placed at a considerable height, requiring a pump to lift the water from underground. An electric motor is used to drive the pump, with IMDs being the preferred choice due to their simplicity and cost-effectiveness. However, it should be noted that IMDs consume a significant amount of reactive power, which can burden the utility grid [1-3], especially during peak demand operations. Therefore, the establishment of standalone WPSs powered by HRESs is an excellent solution to reduce the load demand on the electric grid [1, 4]. Furthermore, it is crucial to develop a seamless control-based WPS that can operate automatically without the need for manual intervention.

Electricity generation using Photovoltaic panels and wind energy systems is widely popular in various locations worldwide. While a WPCS necessitates an electrical generator connected to a turbine for power production,

Photovoltaic panels can directly generate electricity from solar energy through the photoelectric effect. It is important to note that relying solely on a single renewable energy source, be it wind or solar, cannot guarantee a consistent supply of electric power as both are dependent on natural conditions. Fortunately, there are ample suitable locations, such as overhead tanks and apartments, as depicted in Figure 1, where both PVU and WPCS can be installed. To ensure an uninterrupted water supply, it is essential to integrate energy storage devices like BBU into the WPS alongside the HRESs. Hence, the hybrid Battery-PV-wind combination has the capability to provide a consistent and dependable electrical supply to the motor that drives the pump.

The arrangement of the hybrid wind-Photovoltaic systems, as depicted in Figure 1(b), is the most efficient use of space and helps in limiting the size of the wind turbine. This setup also prevents any partial shading effect on the PV panels caused by the wind turbines. Typically, 5-10 hp motors are utilized to lift underground water into overhead tanks or apartments. To ensure a cost-effective setup, an IMD is chosen. In wind generation, a PMDC based generator is selected to minimize losses. Therefore, the proposed configuration is both cost-effective and results in minimal losses. To ensure uninterrupted water supply, a battery bank can be chosen based on the backup requirements. Thus, it is crucial to design the battery bank appropriately for the specific application, considering both the requirements and affordability.

The article is being presented to achieve the below objectives:

^{1,2,3,4,5} Electrical Engineering Department, Vishwakarma Government Engineering College, Chandkheda, Ahmedabad, Gujarat, India.

¹ ORCID ID: 0009-0007-2995-7462, ²0009-0005-3281-3297

³0009-0003-3746-0457, ⁴0009-0003-3945-8182, ⁵0009-0003-7729-1002

⁶Mechanical Engineering Department, Vishwakarma Government Engineering College, Chandkheda, Ahmedabad, Gujarat, India.

⁶ORCID ID: 0009-0004-8578-9537

* Corresponding Author Email: parmar.vaibhavi@gmail.com

- To create a highly efficient hybrid SMS that ensures continuous water supply.
- Creating a central control system to ensure smooth functioning of the WPS.
- To ensure optimal energy management across various sources, loads, and batteries, a control system has been suggested.
- To examine various responses of the WPS under different operating conditions by establishing a HIL setup with OPAL-RT modules.

The document is structured into the subsequent sections. Section-II contains the system description and ratings. The control method proposal can be found in Section-III. The SVC model of induction motor with mathematical expressions is demonstrated in Section-IV. Section-V outlines the HIL based results across different operating conditions. The paper concludes with summary and key references.

The utilization of hysteresis band in traditional DTC implementations results in a fluctuating switching frequency, which is influenced by factors such as rotor speed, load, sample frequency, and more. The fluctuating switching frequency can lead to the emergence of resonant dynamics in loads, thus posing a notable drawback of SVM-DTC.

2. System Description and Ratings

A Hybrid Battery-Wind-PV based SMS for water pumping is presented in Fig. 2. Individual MPPT circuits are connected for WPCS and PVUs to obtain their highest efficiency. The dc-link is established by interconnecting the outputs of all MPPT converters in parallel. A BBU which consists of multiple batteries is connected to dc-link through a dc-to-dc bidirectional circuit. Proper control method is developed for dc-to-dc bidirectional circuit to make a proper discharging and charging process of the BBU. The PMDC type generator in WPCS and IMD for driving the WPS is considered in this paper to make system less loses. The inverter, which is directly linked to the dc-link, operates the IMD. The control mechanism is employed with SoC of the BBU. The majority of motors with a rating of 5-7kW are utilized for the purpose of lifting water from underground sources to overhead tanks. However, the exact rating of a motor is depending on both height of overhead tank/apartment and depth of water. A 5.5kW rating of IMD which listed in Table-1 is considered in this paper to drive the pump. A 4.5kW rating of a PVU [5] and 3.0kW rating of WPCS [6, 7] are considered in this paper to run 5.5kW IMD effectively. Respective parameters of PVU and WPCS are listed in Table-2 and Table-3. The surplus power will be stored in the BBU for later utilization in scenarios where there is inadequate power to operate the IMD. The motor

will be running at constant speed since battery can maintain energy balance in the WPS by regulating voltage at dc-link as per its reference signal. This can be possible by managing discharging and charging of the BBU through dc-to-dc bidirectional circuit. Hence, the dc-link reference voltage is set at 640V, matching the motor's rated voltage (three phase IMD). Seamless operation for the motor is achieved by controlling the inverter show in the Fig. 2. Signals 'A' and 'B' are detected through the utilization of sensors that correspond to the upper (98%) and lower (60%) levels of the tank.

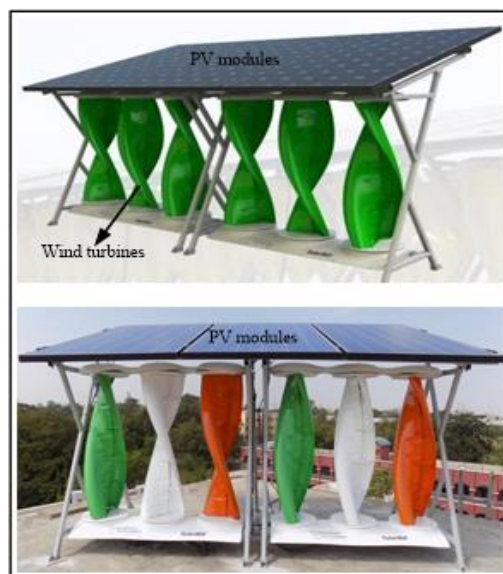


Fig. 1. Hybrid PVU and WPCS

Several scholars have recently preserved comparable WPSs that rely on renewable energy sources. This section highlights a few of these systems. In [1-3], authors have proposed WPS driven by IMDs and powered by PVU. In [5], a novel control technique is presented for a boost zeta converter in a PVU-based WPS. The authors in [6-8] suggested a water pumping system that utilizes PVU and a BLDC motor. However, this system is more expensive due to the use of extra sensors, making it unaffordable for applications such as overhead tanks and apartment tanks. In their study, researchers in [9] introduced a WPS that utilizes a SEPIC converter to enhance system performance even in mismatching conditions. On the other hand, researchers in [10] demonstrated a single stage grid connected WPS powered by a switched reluctance motor. However, it should be noted that this system is specifically designed to be connected to the grid. Additionally, authors in [11] presented a wireless control system for water pumping, which is operated by PVU. Authors in [12-13] have introduced a PVU-based WPS with a storage tank for use in rural areas. In a separate study, authors in [14] have developed a PVU-powered WPS with an automated control system specifically designed for irrigation purposes. The models presented by authors in references [1-3, 5-14] did

not incorporate WPCS. Water pumping systems with wind energy were showcased by authors in references [15-22] for a range of applications. However, numerous authors have neglected to take batteries into account for energy storage. They require additional circuits to operate their motors and lack seamless controls. Hence, a proficient EMS is necessary to create a cohesive system that is better suited for WPSs.

The BBU has the capacity to operate continuously for 24 hours in order to power a 5.0kW motor. This allows it to run for 4-5 days as only a few hours per day are needed to fill the water storage tanks. Typically, the market offers a wide range of 48.0V batteries, therefore the battery bank's Ah rating is approximated at 60% of the initial SoC. To ensure the appropriate voltage (i.e., 192.0V), four batteries with a voltage of 48.0V each are connected in series. The Ah rating of each battery is calculated using the following equation.

$$I_b = (5kW \times 24hr)/(192V \times 0.6) \sim 1050Ah \quad (1)$$

Consequently, all 120Ah rated batteries are taken into consideration. To maintain the rated Ah, a total of 9 battery banks are interconnected in parallel.

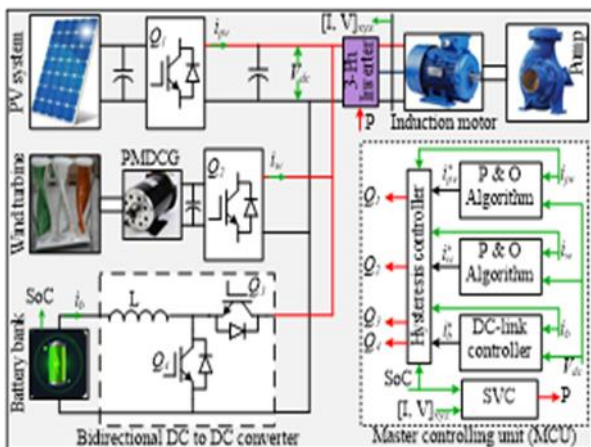


Fig. 2 Proposed HRES based WPS with BBU.

Table 1. Parameters of IMD.

S.No	Parameters	Values
1	Motor power rating (kW).	5.5
2	Rated speed (RPM)	1460
3	Operating frequency (Hz)	50
4	Number of poles	4
5	Operating voltage(V).	380.
6	Stator slots number	48
7	Rotor slots number	40

8	Rated current (A)	10.7.
---	-------------------	-------

Table 2. Parameters of PVU.

S.No	Parameters/Module	Values
1	Power (W)	300.
2	Voltage at open circuit (V).	45.7.
3	Short circuit current (A).	8.55.
4	Voltage at maximum power (V).	37.5.
5	Current at maximum power (A).	7.99.
6	Series modules/Array.	5.0
7	Number of parallel arrays.	3.0
8	Maximum power of PVU (kW).	4.50.

Table 3. Parameters of WPCS (PMDC).

S.No	Parameters	Values
1	Type of generator.	Vertical
2	Power(kW).	3.0.
3	Maximum Power(kW).	4.0.
4	Operating wind speed(m/s).	12.0.
5	Cutoff speed(m/s).	2.8.
6	Safety wind speed(m/s).	50.0.
7	Output DC voltage(V).	120.
8	Maximum speed (rpm) by rotor.	240.

3. Proposed Seamless Control for EMS

The fluctuating atmospheric conditions cause the electrical power generated by WPCS and PVU to be inconsistent. To ensure a stable energy balance between generation and load (such as a motor), fast energy storage devices, such as batteries, are integrated. These batteries help regulate the voltage at the dc-link. Additionally, PVU and WPCS are equipped with individual MPPT converters and their respective P&O algorithms. The P&O technique was designed to minimize the number of sensors by utilizing the dc-link voltage, eliminating the need to sense voltage at the PVU and WPCS. In order for the IMD to operate at a constant speed, an effective control method was necessary, leading to the integration of SVC in the WPS. The TS-Fuzzy

controller generates the reference current (i_{ref}) of BBU by utilizing the voltage difference between the actual and reference signal (i.e., 640V) at the dc-link. The necessary pulses are being generated for the DC-to-DC circuit switches (Q3 and Q4) by utilizing a hysteresis current loop that compares the actual and reference currents of BBU. In order to avoid excessive charging and discharging of the BBU, switches are integrated with the SoC signal. The minimum SoC level is set at 5% (0.05), while the maximum limit is set at 95%. When the battery's SoC reaches the upper limit, the charging switch (Q3) is turned off. To maintain power balance, the PVU and WPCS deactivate their MPPT converters and perform deloading operations. If the SoC falls below the lower threshold, it is necessary to deactivate the discharging switch and simultaneously disconnect the motor from the DC-link by opening the inverter switches. After disconnecting the motor from the dc-link, the BBU will commence charging.

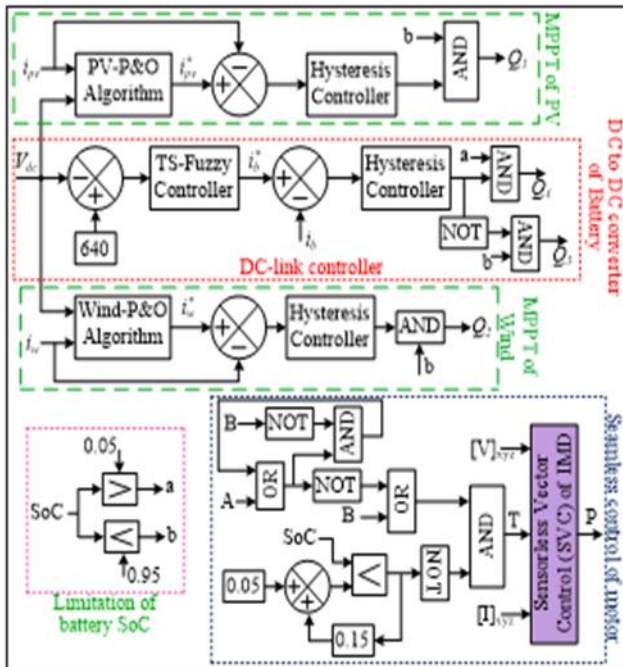


Fig. 3. Proposed seamless controller.

In order to avoid frequent motor activation and deactivation, the motor will be turned on again via the inverter once the SoC of BBU reaches 20%, provided that the water level in the tank has not yet reached its higher level of 98%. Upon reaching the maximum water level (where Signal A is indicated as '1'), the motor will cease operation automatically, irrespective of the charge status. Nevertheless, in order to prevent the motor from frequently turning on and off when the water level drops below its upper limit ($A = '1'$), the control method will delay switching on the motor until the water level decreases to its lower threshold B ($B = '1'$ if the water level falls below 60.0% of the tank capacity). Consequently, the recommended unified control method is able to manage the motor-pump set utilizing both SoC and water level (B and

A as indicated in Figure 6 in the results section). The illustrated unified master control methodology is displayed in Figure 3. Details of TS-Fuzzy controller are provided in Appendix.

4. Sensorless Vector Control of Induction Motor

The authors in [11, 34] introduced a water pumping system that relies on scalar control of IMD. Nevertheless, it is important to note that scalar control (v/f) has a constraint where the voltage cannot exceed the rated value. Consequently, this limitation also restricts the frequency from surpassing the rated value for the applications of constant torque. Implementing the constant v/f technique on an IMD, is straightforward but results in slow response due to the coupling effect caused by flux and torque being dependent on current and frequency. Additionally, achieving precise position control is unattainable with scalar control as it necessitates immediate torque control. Conversely, vector control separates the field current and armature flux vectors, allowing for independent control to achieve rapid transient response. The currents of the 3-phase motor are segregated into two components: the field (I_d) and the torque (I_q). In this scenario, the resulting torque can be represented as stated in reference [27].

$$T_e = K I_d I_q \quad (2)$$

The term I_d is aligned with the flux (Ψ) while I_q is positioned perpendicular to it. Consequently, regulating the reference current of I_q impacts solely the I_q current, leaving the flux unaffected. Likewise, when the reference current of I_d is regulated, it solely manages the flux and has no impact on the I_q current component [27]. In this study, as we maintain I_d constant to control I_q , the flux will stay consistent across different operational scenarios.

The motor torque in a water pumping system is determined by the head, while the load torque remains constant for a constant head. With a constant load torque, the power required by the load is solely dependent on the motor's speed. Consequently, any disparity between the load power and the generated power will result in a change in speed. Similarly, when the PV power exceeds or falls short of the load requirement, the dc-link voltage (V_{dc}) will correspondingly increase or decrease. To maintain a constant output voltage for AC buses (i.e., the inverter's output connected to motor loads), it is necessary to regulate the V_{dc} at 640V. Therefore, in the suggested control approach, the permissible limits enable the variation of the speed of IMD while maintaining a constant dc-link voltage. Figure 4 illustrates the SVC implemented with TS-Fuzzy controllers. Given that the frequency of the inverter is variable, it directly affects the speed of the IMD. Consequently, in order to ensure the motor operates safely and reliably, the controller permits the IMD (Integrated Motor Drive) to function within the acceptable range of

minimum and maximum speeds. By considering a head of 25m and a maximum water discharge (Q) of 300 gal/min, the minimum and maximum speeds of the IMD can be determined through calculation. The allowable velocity (restricted by a limiter) serves as the input signal for the SVC, which then produces the necessary pulses (P1-6) for the inverter.

The speed can be estimated by the following equations [25]:

$$v_{ds}^s = i_{ds}^s R_s + L_{ls} \frac{d}{dt} (i_{ds}^s) + \frac{d}{dt} (\Psi_{dm}^s) \quad (3)$$

$$v_{ds}^s = L_m/L_r \frac{d}{dt} (\Psi_{dr}^s) + (R_s + \sigma L_s S) i_{ds}^s \quad (4)$$

Where $\sigma = 1 - (L_m^2)/(L_r L_s)$

$$\frac{d}{dt} (\Psi_{dr}^s) = L_r/L_m v_{ds}^s - L_r/L_m (R_s + \sigma L_s S) i_{ds}^s \quad (5)$$

Similarly:

$$\frac{d}{dt} (\Psi_{qr}^s) = L_r/L_m v_{qs}^s - L_r/L_m (R_s + \sigma L_s S) i_{qs}^s \quad (6)$$

$$\frac{d}{dt} (\Psi_{dr}^s) = L_m/L_r i_{ds}^s - \omega_r \Psi_{qr}^s - 1/T_r \Psi_{dr}^s \quad (7)$$

$$\frac{d}{dt} (\Psi_{qr}^s) = L_m/L_r i_{qs}^s - \omega_r \Psi_{dr}^s - 1/T_r \Psi_{qr}^s \quad (8)$$

Where, $T_r = L_r/R_r$ Moreover, the rotor angle can be achieved by the following expression:

$$\theta_e = \tan^{-1} \left[\frac{(\Psi_{qr}^s)}{(\Psi_{dr}^s)} \right] \quad (9)$$

Hence, the rotor speed is calculated by:

$$\omega_r = \frac{d}{dt} \theta_e =$$

$$\frac{1}{(\Psi_r^2)} \left[(\Psi_{dr}^s \frac{d}{dt} \Psi_{qr}^s - \Psi_{qr}^s \frac{d}{dt} \Psi_{dr}^s) - L_m/T_r (\Psi_{dr}^s i_{qs}^s - \Psi_{qr}^s i_{ds}^s) \right] \quad (10)$$

Slip speed can be estimated as follows:

$$\omega_{slip} = ((1 + \sigma T_r S) L_s i_{qs}) / (T_r (\Psi_{ds} - \sigma L_s i_{ds})) \quad (11)$$

Therefore, one can approximate the velocity of IMD:

$$\omega = \omega_{slip} + \omega_r$$

(12)

C speed (ω) will be compared to reference speed (ω^*). The error will be given to the TS-Fuzzy controller and it will produce reference quadrature axis current (i_{q}^*) with the help of flux. The reference current of the direct axis (i_{d}^*) can be estimated from flux reference value. Pulses for inverter are generated from PWM generator with the help of reference currents as shown in Figure 4.

5. HIL Based Results

The suggested system has been evaluated through the utilization of HIL on the OPAL-RT platform. To create the HIL, two modules of OPAL-RTs are linked in a series. The system being tested is situated in OPAL-RT-1, while the proposed control method is placed in OPAL-RT-2. Figure 4 illustrates the laboratory configuration of HIL. The outcomes are demonstrated in the system and presented in this section. The comprehensive HIL configuration of the suggested system (Figure 2) can be seen in Figure 5, showcasing suitable color coordination.

Additionally, Figure 5 includes the upper ('A') and lower ('B') level points of the water tank, which are not visible in Figure 2. The 'A' signal will change to '1' when the water level reaches its maximum limit (98%), while the 'B' signal will switch to '1' when the water level drops below 60% of the tank capacity. The results obtained are displayed on a different computer instead of an oscilloscope for improved visualization. The system parameters and components design are based on references [23-27].

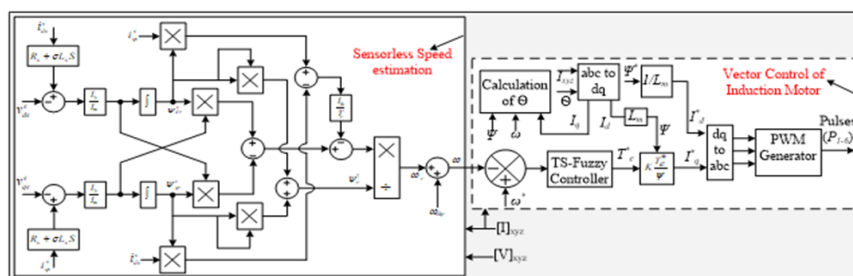


Fig. 4. HIL configuration block.

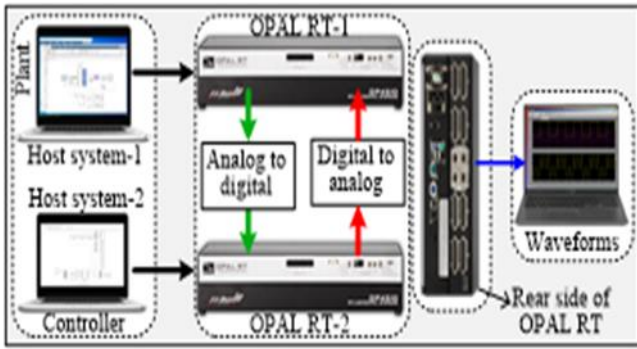


Fig. 5. HIL configuration block.

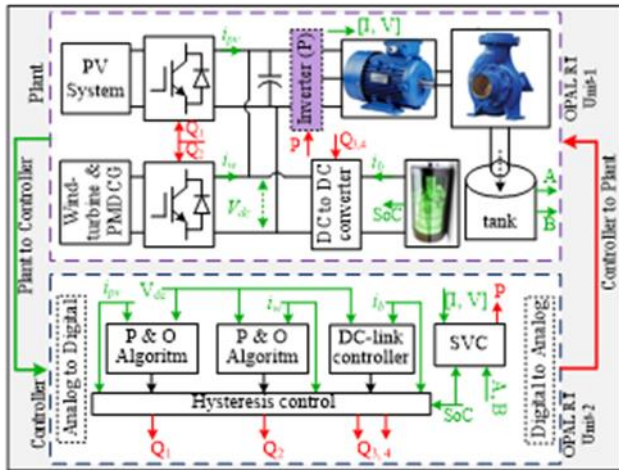


Fig. 6. HIL model of proposed WPS.

Consider the drop in irradiance from 1000 to 400W/m² at $t=2.0$ sec, followed by an increase from 400 to 700W/m² at $t=4.0$ sec while operating the motor to drive the pump. Simultaneously, there is a change in wind speed from 12.0m/s to 7m/s at $t=3.0$ sec. The water tank is expected to reach its full capacity at $t=6$ seconds ($A=1$). The changes mentioned above are visually represented in Figure 7. Throughout this process, the suggested controller effectively manages energy as demonstrated in Figure 8. The power produced by the PVU and WPCS fluctuates in response to changes in wind speed and solar irradiance. The wind turbine power diminishes gradually as the speed of the wind turbine decreases, as a result of a two-mass drive train being taken into account in this study. Nevertheless, the power consumed by the motor remains constant until the tank level reaches its maximum capacity (i.e., $A=1$). Consequently, the BBU is reacting to the imbalance between the total generation and motor load. Once the motor automatically shuts off (at $t=6.0$ sec), the excess power generated by both the PVU and WPCS is efficiently utilized by the battery through the management of the bidirectional dc to dc circuit.

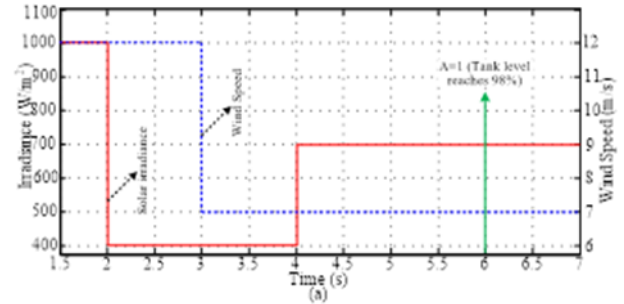


Fig. 7. Variations in wind speed, solar irradiance, and level of water tank (i.e., signal of 'A').

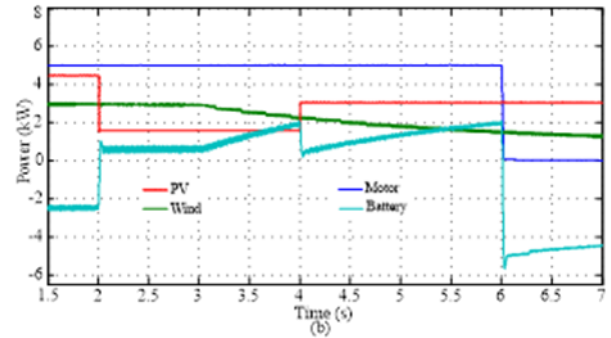


Fig. 8. Various powers.

The bidirectional circuit regulates the DC-link voltage at a reference value of 640V to control the charging and discharging of the battery, thereby determining the speed of the motor. The DC-link voltage is shown in Figure 9(a) at a fixed value of 640V. The State of Charge (SoC) of the battery is illustrated in Figure 9(b). Upon examination of Figure 9(b), it is evident that the battery charging and discharging process is clearly illustrated in correlation to the battery power response shown in Figure 8.

The ascending line signifies the battery charging (increasing State of Charge), while the descending line represents the battery discharging mode. The water level within the tank will gradually increase until it reaches the upper-level indicator, triggering the automatic shutdown of the motor by the seamless controller. The tank will then maintain a constant level until water is discharged from the outflow. The water level and corresponding operating points are shown in Figure 9(c).

The control decision will be based on the tank level and SoC of the BBU. As a result, the motor will operate continuously at a constant speed until the water tank reaches its upper level or until the battery has adequate storage capacity. It is important to note that the voltage reference signal is set at 640V, which corresponds to the rated voltage of the motor at a speed of 157 RPS. The speed of the motor can be adjusted by modifying the reference voltage signal of the DC-to-DC circuit. As a result, the motor will run at a constant speed of 157 RPS until it halts when the letter 'A' changes to '1'. This ensures smooth operation of the system. The cycle continues until the user inputs new reference

signals, as the system is intended to be user-friendly.

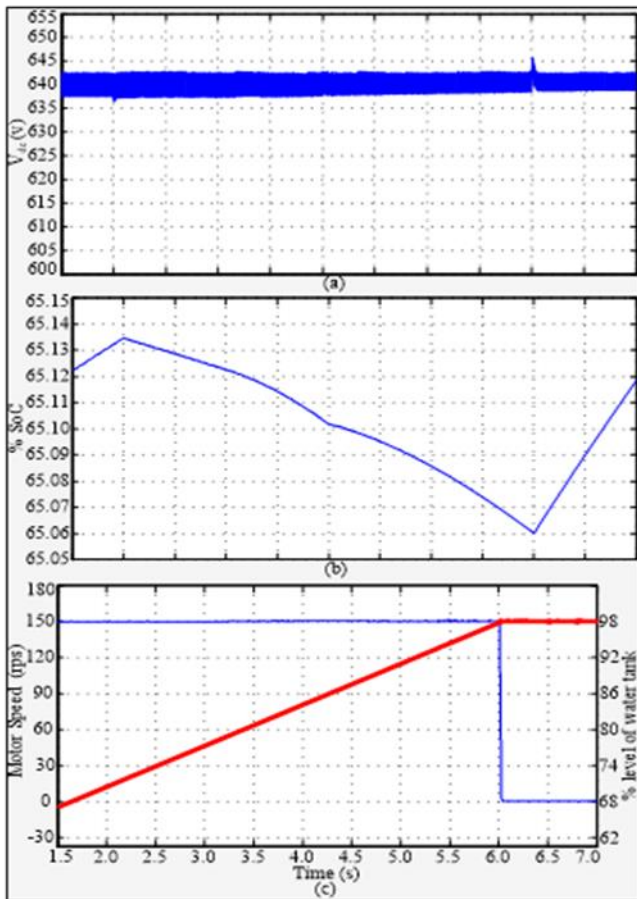


Fig. 9. (a) Voltage at DC-link, (b) SoC of the BBU, (c) IMD speed (blue color) and water level in tank.

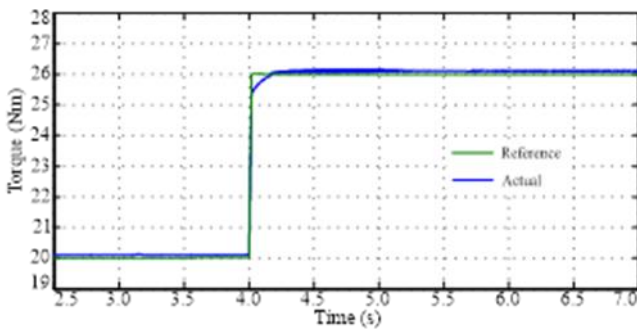


Fig. 10. Torques of IMD.

Similarly, sometimes needs to be operating IMD at various speeds especially in aqua farms. Hence, the proposed WPS is tested for changing reference speed from 1400 to 800 RPM. The response under this situation is shown in Figure 11. The actual motor speed is always following the reference by proposed control strategy.

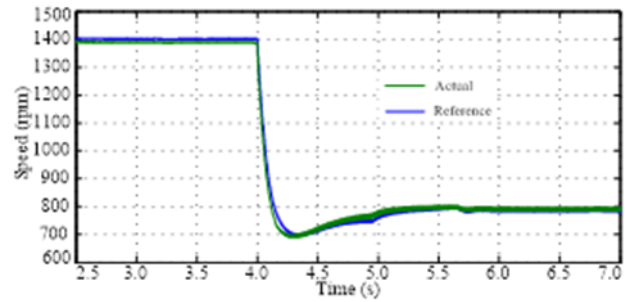


Fig. 11. Speed responses of IMD.

6. Conclusion

In this paper, a well-designed EMS and an innovative controller are presented for a WPS that utilizes PVU, WPCS, and BBU as energy sources. The controller operates automatically, considering the SoC and the water level in the tank. Since the power generation from WPCS and PVU is subject to fluctuations, a bidirectional DC to DC converter is employed to regulate the battery operation accordingly. An SVC is developed on IMD to drive the water pump. Instead, the motor's speed can be adjusted to meet our needs by modifying the reference voltage signal of the DC-to-DC circuit controller. To implement this system, HIL is utilized with the assistance of OPAL-RT devices. The results of this study are then displayed using a PC connected to the HIL interface. Satisfactory outcomes are achieved and demonstrated across different scenarios in this research paper.

References

- [1] C. N. Bhende and S. G. Malla, "Novel control of photovoltaic based water pumping system without energy storage", *International Journal of Emerging Electric Power Systems*, Vol. 13, Issue 5, Nov. 2012.
- [2] S. G. Malla, C. N. Bhende and S. Mishra, "Photovoltaic based water pumping system", *IEEE: International Conference on Energy, Automation and Signal*, India, Dec. 2011.
- [3] Saurabh Shukla and Bhim Singh, "Reduced-Sensor-Based PV Array-Fed Direct Torque Control Induction Motor Drive for Water Pumping", *IEEE Transactions on Power Electronics*, Vol. 34, Issue: 6, pp. 5400-5415, June 2019.
- [4] M. N. Ibrahim, H. Rezk, M. Al-Dhaifallah and P. Sergeant, "Solar Array Fed Synchronous Reluctance Motor Driven Water Pump: An Improved Performance Under Partial Shading Conditions", *IEEE Access*, vol. 7, pp. 77100-77115, 2019.
- [5] Meghna and Y. K. Chauhan, "PV Water Pumping Using Integrated Quadratic Boost Zeta Converter," *2018 International Conference on Power Energy, Environment and Intelligent Control (PEEIC)*, 2018, pp. 120-125, doi: 10.1109/PEEIC.2018.8665640.

- [6] A. K. Wankhede, S. Pal, M. Singh, O. R. Gogte, A. Sharma and B. G. Fernandes, "Development of Efficient 5-HP BLDC motor for Solar water pump and performance comparison with Induction Motor counterpart," 2021 IEEE India Council International Subsections Conference (INDISCON), 2021, pp. 1-4, doi: 10.1109/INDISCON53343.2021.9582231.
- [7] S. G. Malla et al., "Whale Optimization Algorithm for PV based Water Pumping System Driven by BLDC Motor Using Sliding Mode Controller," in IEEE Journal of Emerging and Selected Topics in Power Electronics, doi: 10.1109/JESTPE.2022.3150008.
- [8] G. S. Chandrakant and S. K. Patil, "Designing of Controller for BLDC Driven Solar Water Pump," 2021 6th International Conference on Inventive Computation Technologies (ICICT), 2021, pp. 390-393, doi: 10.1109/ICICT50816.2021.9358629.
- [9] A. Tomar, P. H. Nguyen and S. Mishra, "SEPIC-MISO Converter Based PV Water Pumping System- An Improved Performance Under Mismatching Conditions," 2020 IEEE 9th Power India International Conference (PIICON), 2020, pp. 1-5, doi: 10.1109/PIICON49524.2020.9112907.
- [10] P. N. Dheeraja and E. S. Prasad, "Grid Interfaced Single Stage Solar Water Pump Using SRM," 2021 6th International Conference on Communication and Electronics Systems (ICES), 2021, pp. 131-137, doi: 10.1109/ICES51350.2021.9489110.
- [11] A. Waleed et al., "Solar (PV) Water Irrigation System with Wireless Control," 2019 International Symposium on Recent Advances in Electrical Engineering (RAEE), 2019, pp. 1-4, doi: 10.1109/RAEE.2019.8886970.
- [12] L. Nabila, F. Khaldi and M. Aksas, "Design of photo voltaic pumping system using water tank storage for a remote area in Algeria," 2014 5th International Renewable Energy Congress (IREC), 2014, pp. 1-5, doi: 10.1109/IREC.2014.6826981.
- [13] A. Bekraoui, M. Yaichi, M. Allali, A. Taybi and A. Boutadara, "Performance of Photovoltaic Water Pumping System in Adrar, Algeria," 2018 6th International Renewable and Sustainable Energy Conference (IRSEC), 2018, pp. 1-5, doi: 10.1109/IRSEC.2018.8702990.
- [14] R. K. Megalingam and V. V. Gedela, "Solar powered automated water pumping system for eco-friendly irrigation," 2017 International Conference on Inventive Computing and Informatics (ICICI), 2017, pp. 623-626, doi: 10.1109/ICICI.2017.8365208.
- [15] H. A. Rabab'ah and Y. N. Anagreh, "Modeling and Simulation of Standalone WECS-PMSG for Water Pumping System," 2021 IEEE PES/IAS PowerAfrica, 2021, pp. 1-5, doi: 10.1109/PowerAfrica52236.2021.9543189.
- [16] M. Saputra, A. Syuhada and R. Sary, "Study of Solar and Wind Energy Using as Water Pump Drive-Land for Agricultural Irrigation," 2018 4th International Conference on Science and Technology (ICST), 2018, pp. 1-4, doi: 10.1109/ICSTC.2018.8528643.
- [17] A. K. Traoré, A. Cardenas, M. L. Doumbia and K. Agbossou, "Comparative Study of Three Power Management Strategies of a Wind PV Hybrid Stand-alone System for Agricultural Applications," IECON 2018 - 44th Annual Conference of the IEEE Industrial Electronics Society, 2018, pp. 1711-1716, doi: 10.1109/IECON.2018.8591683.
- [18] A. Saidi, A. Harrouz, I. Colak, K. Kayisli and R. Bayindir, "Performance Enhancement of Hybrid Solar PV-Wind System Based on Fuzzy Power Management Strategy: A Case Study," 2019 7th International Conference on Smart Grid (icSmartGrid), 2019, pp. 126-131, doi: 10.1109/icSmartGrid48354.2019.8990675.
- [19] W. Obaid, A. Hamid and C. Ghenai, "Hybrid MPPT Controlled Solar/Wind Power System for Pumping System," 2019 International Conference on Electrical and Computing Technologies and Applications (ICECTA), 2019, pp. 1-4, doi: 10.1109/ICECTA48151.2019.8959772.
- [20] W. Obaid, A. Hamid and C. Ghenai, "Hybrid Solar/Wind/Diesel Power System for Water Pumping Application," 2019 7th International Renewable and Sustainable Energy Conference (IRSEC), 2019, pp. 1-6, doi: 10.1109/IRSEC48032.2019.9078183.
- [21] Z. Mousavi, R. Fadaeinedjad, H. Moradi, M. Bagherzadeh and G. Moschopoulos, "A New Configuration for Wind/Solar Water Pumping System Based on a Doubly Fed Induction Generator," 2020 IEEE Energy Conversion Congress and Exposition (ECCE), 2020, pp. 1891-1898, doi: 10.1109/ECCE44975.2020.9235941.
- [22] A. Nekkache, B. Bouzidi, M. S. A. Cheikh, Y. Bakelli, A. Kaabeche And A. Dali, "Optimal Sizing Of Hybrid PV/Wind Based Water Pumping System Considering Reliability And Economic Aspects," 2018 International Conference on Wind Energy and Applications in Algeria (ICWEAA), 2018, pp. 1-6, doi: 10.1109/ICWEAA.2018.8605087.
- [23] J. K. Singh, K. A. Jaafari, R. K. Behera, K. A. Hosani and U. R. Muduli, "Faster Convergence Controller With Distorted Grid Conditions for Photovoltaic Grid Following Inverter System," in IEEE Access, vol. 10,

pp. 29834-29845, 2022, doi:
10.1109/ACCESS.2022.3159476.

- [24] O N Chandrasekhar, "Modified Grey Wolf Optimization Algorithm for MPPT of PV System under Partial Shading Conditions", *International Journal of New Technologies in Science and Engineering (IJNTSE)*, Vol. 8, Issue. 5, pp. 1-6, May. 2022.
- [25] A. Dash, D. P. Bagarty, P. K. Hota, U. R. Muduli, K. A. Hosani and R. K. Behera, "Performance Evaluation of Three-Phase Grid-Tied SPV-DSTATCOM With DC-Offset Compensation Under Dynamic Load Condition," in *IEEE Access*, vol. 9, pp. 161395-161406, 2021, doi: 10.1109/ACCESS.2021.3132549.
- [26] Priyanka Malla, "Novel Control Technique for MPPT of PV Standalone System with TSK Fuzzy controller", *International Journal of New Technologies in Science and Engineering (IJNTSE)*, Vol. 8, Issue. 8, pp. 1-7, Aug. 2022.
- [27] U. R. Muduli, K. A. Jaafari, K. A. Hosani, R. K. Behera, R. R. Khusnutdinov and A. R. Safin, "Cell Balancing of Li-ion Battery Pack with Adaptive Generalised Extended State Observers for Electric Vehicle Applications," 2021 *IEEE Energy Conversion Congress and Exposition (ECCE)*, 2021, pp. 143-147, doi: 10.1109/ECCE47101.2021.9595601.